$(Fe,Co)_2(P,Si)$ rare-earth free permanent magnets

From macroscopic single crystals to submicron-sized particles

Yibole, H.; Lingling-Bao, B.; Xu, J. Y.; Alata, H.; Tegus, O.; Hanggai, W.; van Dijk, N. H.; Brück, E.; Guillou, F.

DOI
10.1016/j.actamat.2021.117388

Publication date
2021

Document Version
Accepted author manuscript

Published in
Acta Materialia

$(Fe,Co)_2(P,Si)$ rare-earth free permanent magnets: from macroscopic single crystals to submicron-sized particles

H. Yibole[1], Lingling-Bao[1], J.Y. Xu[1], H. Alata[1], O. Tegus[1], W. Hanggai[2], N. H. van Dijk[2], E. Brück[2], F. Guillou[1,*]

1- Inner Mongolia Key Laboratory for Physics and Chemistry of Functional Materials, Inner Mongolia Normal University, Hohhot, 010022, China

2- FAME group, Department of Radiation Science & Technology, Delft University of Technology, Mekelweg 15, 2629JB Delft, The Netherlands

* Inner Mongolia Key Laboratory for Physics and Chemistry of Functional Materials, Inner Mongolia Normal University, 81 Zhaowuda Road, Hohhot, 010022, China; E-mail address: francoisguillou@imnu.edu.cn (F. Guillou).

Abstract

While rare-earth magnets exhibit unchallenged hard-magnetic properties, looking for alternatives based on inexpensive elements of non-critical supply remains of utmost interest. Here, we demonstrate that $(Fe,Co)_2(P,Si)$ single crystals combine a large magnetocrystalline anisotropy (K_1 ≈ 0.9 MJ m^{-3} at 300 K), high Curie temperatures (T_C up to 560 K) and an appreciable saturation specific magnetization (101 A m^2 kg^{-1}) leading to a theoretical $|BH|_{max}$ ≈ 165 kJ m^{-3}, making them promising candidate materials as rare-earth-free permanent magnets. Our comparison between $(Fe,Co)_2P$ and $(Fe,Co)_2(P,Si)$ single crystals highlights that Si substitution reduces the low-temperature magnetocrystalline anisotropy, but strongly enhances T_C, making the latter quaternary alloys most favorable for room temperature applications. Submicron-sized particles of $Fe_{1.75}Co_{0.20}P_{0.75}Si_{0.25}$ were prepared by a top-down ball-milling approach. While the energy products of bonded particles are to this point modest, they demonstrate that permanent magnetic

properties can be achieved in $(Fe,Co)_2(P,Si)$ quaternary alloys. This work correlates the development of permanent magnetic properties to a control of the microstructure. It paves the way toward the realization of permanent magnetic properties in $(Fe,Co)_2(P,Si)$ alloys made of economically competitive Fe, P and Si elements, making these materials desirable for applications.

Keywords: Magnetism, Magnetic properties, Single crystal, Nanomaterials.

1. Introduction

Permanent magnets have become indispensable components of many mass-market consumer and industrial products, including applications in motors, generators and actuators. Nowadays, two families of magnets are produced on a large scale. The ferrite family, with the most common phases being $BaFe_{12}O_{19}$ and $SrFe_{12}O_{19}$, are cheap and relatively easy to produce magnets, but their figure of merit, the energy product $|BH|_{max}$ is limited, of the order of 44 kJ m^{-3}. On the other hand, rare-earth permanent magnets are high-performance magnets and represent about 2/3 of the permanent magnet market in monetary value [1]. The most well-known are Nd-Fe-B magnets, which can present energy products as high as 500 kJ m^{-3}. Nd-Fe-B is a very high-performance magnet, as it is largely made of iron and appropriate magnetic hysteresis can be maintained at temperatures up to 200 °C by replacing Nd by heavy rare earths, Dy or Tb. Unfortunately, the criticality of the supply of heavy rare earths forces attention to be paid to the possibilities of replacing, or at least reducing the cost production and recycling of these magnets [2-5]. Therefore, developing new, cost-competitive, rare-earth-free materials with a maximum energy product lying in the gap between ferrite and rare-earth magnets is of primary importance [4]. Such a material could enhance the performance and reduce the weight of devices that currently use ferrites, or greatly reduce the cost of devices that currently use rare-earth magnets. Several 3*d* transition metal based materials families are considered as potential rare-earth-free permanent magnets, including MnBi, MnAl, Mn_2Ga, $Fe_{16}N_2$, YCo_5, FePt, CoPt [3-6]. But, despite intense research and the achievement of interesting properties, no clear preferred candidate emerges at present.

In this context the Fe_2P materials family is worth considering. The parent binary alloy is made by nearly 80 wt.% of iron, the most abundant magnetic element on earth, ensuring easy supply and a reasonable cost. Fe_2P also presents a reasonably large saturation magnetic polarization (J_s = $\mu_0 M_s \approx 1.05$ T at 5 K) and a uniaxial magnetic anisotropy with the hexagonal *c* axis being the easy magnetic axis [7-9]. These later two properties are essential in view of realizing permanent

magnets. Its magneto-crystalline anisotropy energy is particularly large, stronger than most of the *3d* based alloys mentioned above. However, its low Curie temperature of T_C = 214 K is incompatible with applications. By substitution of Fe by Co, De Vos *et al.* reported in 1962 an increase in Curie temperature and the possibility to prepare permanent magnets with a coercive field $\mu_0 H_c$ of about 0.2 T at room temperature [10]. Further attempts at developing permanent magnets deriving from Fe_2P have however been impeded by the appearance of a competing orthorhombic crystal structure in $Fe_{2-y}Co_yP$ ternary alloys when y reaches 0.3 [11]. Substituting Ni for Fe is also known to increase the Curie temperature, but at the expense of a reduction in both magnetic anisotropy and saturation magnetization [12]. Similarly, substitutions of P for other metalloid such as Si, As, Ge, or B raise T_C, but also result in the appearance of competing crystal structures [13-15]. At the end, it turned out difficult to optimize ternary alloys deriving from Fe_2P for permanent magnet applications. Even though significant advances have been made to prepare $Fe_{2-y}Co_yP$ in nanosized form, the relatively large coercive field of $\mu_0 H_c$ = 0.57 T at 5 K of such small nanoparticles quickly vanishes as the blocking temperature of these superparamagnetic particles is relatively low [16-19].

Several theoretical studies have clarified the origin of the large magneto-crystalline anisotropy in Fe_2P and related alloys, which in particular highlighted the strong dependence of the magnetic properties on both the band filling and structural distortions affecting the *c/a* ratio of the hexagonal lattice parameters [20,21]. It led to the prediction of the possibility to maintain a strong magneto-crystalline anisotropy of Fe_2P in quaternary alloys by simultaneous substitutions on the metal and metalloid sites [22]. Yet more experimental insights are needed, in particular as the stability range of the hexagonal structure is virtually unknown in quaternary alloys deriving from Fe_2P, except for $(Mn,Fe)_2(P,As)$, $(Mn,Fe)_2(P,Ge)$ or $(Mn,Fe)_2(P,Si)$ studied for their giant magnetocaloric effect [23-26]. Preliminary experimental studies in polycrystalline $Fe_{2-y}Co_yP_{1-x}Si_x$ and $Fe_{2-y}Ni_yP_{1-x}Si_x$ allowed us to roughly estimate the chemical compositions for which the hexagonal Fe_2P-type structure

can be observed, and an oriented powder method suggested the possibility to combine high Curie temperatures and strong magnetic anisotropy with *c* as easy axis [27,28]. However, two main issues remained to be tackled, prior to quaternary compounds deriving from Fe_2P could be truly considered as potential rare-earth-free permanent magnets. First, a more accurate determination of the magneto-crystalline anisotropy constants than that obtained in oriented $Fe_{2-y}Co_yP_{1-x}Si_x$ polycrystalline materials is needed. Ideally, this requires single crystals. While the growth of binary Fe_2P and ternary $Fe_{2-y}Ni_yP$ single crystals has been reported a few decades ago [7,12], that of quaternary alloys containing Si is highly challenging due to the combination of a high volatility of P and a low solubility of Si in the flux. The growth of ferromagnetic quaternary alloys deriving from Fe_2P has seldom been successful; So far, only in $Fe_{2-y}Mn_yP_{1-x}Si_x$ magnetocaloric materials with low T_C or with antiferromagnetic order, *i.e.* with a limited Si content [29]. The second aspect requiring attention is that $Fe_{2-y}Co_yP_{1-x}Si_x$ polycrystalline materials do not show coercivity nor remanence in bulk form after synthesis by solid state reaction. As demonstrated here, developing appropriate microstructures is beneficial to turn the large magnetic anisotropy into true hard magnetic properties.

2. Experimental Methods

2.1 Single crystals synthesis

$Fe_{2-y}Co_yP$ and $Fe_{2-y}Co_yP_{1-x}Si_x$ single crystals were grown by the flux method with tin as a metallic flux. Several batches were synthesized to obtain the targeted Co and Si compositions. High-purity Co (99.9%), Fe (99.9%), P (97.3%), and Si (99.999%) were used as starting materials. The starting materials were mixed with high-purity Sn (99.99%) and then arc-melted under an Ar atmosphere in water-cooled copper crucible. The resulting ingot was then sealed in a quartz ampoule in an Ar atmosphere of 200 mbar. The charge to flux ratio was 1:20 wt. %. The sealed ampoules were placed in a vertical furnace and heated to 1473 K over 10 h, then maintained at this temperature for 100 h, and later cooled at a rate of 2.5 K h^{-1} to 900 K at which temperature

the excess of tin was removed. The remaining flux was removed by etching with diluted hydrochloric acid.

2.2 Submicron-sized particles synthesis

$Fe_{1.75}Co_{0.20}P_{0.8}Si_{0.2}$ submicron-sized particles were produced by a two-stage process. First, bulk polycrystalline materials are prepared by mechanical alloying (planetary Fritsch Pulverisette) of elemental starting materials during 10 h using a ball:sample weight ratio of 5:1 followed by shaping into pellet and a solid state reaction at 1100 °C during 24 h ending by a quenching. The resulting bulk polycrystalline samples mainly consist of the main Fe_2P-type phase (about 95 wt.%, with some contamination from secondary phase having 3:1 or 5:3 metal:metalloid ratio depending on Si content) and are well crystallized with an average grain size of the order of 40 µm. At the second step, submicron-sized particles are produced by ball-milling (ball:sample mass ratio 6:1 in stainless steel jars with balls of 4 g) either using dry milling or surfactant assisted wet milling with Heptane (99.8% purity) as solvent with 20 wt.% oleic acid (90 % purity) as surfactant. The jars were sealed under purified Ar atmosphere. Different milling times were used.

2.3 Chemical and physical characterizations

The morphology and chemical composition of the single crystal were determined by scanning electron microscopy (SEM, Hitachi SU8010 and Hitachi TM3030Plus) and energy-dispersive X-ray spectroscopy (EDS, using an acceleration voltage of 15 keV). To get a more quantitative estimate of chemical compositions, polycrystalline $Fe_{1.00}Si_{1.00}$ and monocrystalline $Fe_{2.00}P_{1.00}$ references were used.

An Empyrean PANalytical diffractometer employing Cu-K radiation was used for powder x-ray diffraction with the internal parameters of the PIXcel detector adjusted to reduce the fluorescence background. For polycrystalline materials, structural refinements were carried out using the

Rietveld method and Fullprof software to confirm the phase content [30]. The VESTA software was used for structure visualization [31].

Magnetic measurements were carried out using a Quantum Design Versalab system equipped with a vibrating sample magnetometer option. For calculation of the anisotropy constant, the demagnetizing field was corrected assuming the internal field $H_{in} = H_0 - NM$, where H_0 is the applied field, M the volume magnetization and N the demagnetizing factor calculated for each crystal using the Osborn tables. In practice the demagnetizing field correction is mostly needed for measurements with the applied field perpendicular to the long axis of the crystal as the demagnetizing factor in this configuration are of the order of 0.45-0.47, close to the value of N = 1/2 expected for an infinitively long needle. For magnetic measurements above 400 K a Lakeshore 7407 vibrating sample magnetometer was used in combination with an electromagnet and a high temperature furnace model 74034 using BN crucibles.

3. Results and discussion

3.1 Growth of $Fe_{2-y}Co_yP_{1-x}Si_x$ single crystals

Several batches of $Fe_{2-y}Co_yP_{1-x}Si_x$ single crystals were grown with a focus on the composition range $0.1 \leq y \leq 0.5$ and $0.2 \leq x \leq 0.4$, respectively. From our preliminary study on polycrystalline samples these compositions appeared the most likely to yield a high T_C and a strong magnetic anisotropy [27]. Simultaneous Co for Fe and Si for P substitutions are required to ensure that the crystal structure is of the hexagonal Fe_2P-type at large Si content, the latter being essential to reach high Curie temperatures. Ternary $(Fe,Co)_2P$ single crystals were also grown to serve as comparative examples. As the flux growth method leads to a certain dispersion of the crystal compositions with respect to the nominal ones, the compositions of the crystals were systematically established using scanning electron microscopy (SEM) coupled with energy dispersive X-ray spectroscopy (EDS) assisted by appropriate references. **Figure 1** presents two

typical crystals: a quaternary $Fe_{1.94\pm0.06}Co_{0.10\pm0.01}P_{0.61\pm0.02}Si_{0.33\pm0.01}$ and a ternary $Fe_{1.78\pm0.04}Co_{0.23\pm0.01}P_{0.98\pm0.02}$ crystal. Both crystals have a prismatic elongated needle-like shape similar to the shape previously observed in hexagonal MnFe(P,Si) single crystals [29]. The surfaces of the crystals are regular and of homogeneous composition. The ternary crystal has dimensions of about $0.13\times0.13\times0.8$ mm^3 and its chemical composition $Fe_{1.78}Co_{0.23}P_{0.98}$ is close to the nominal starting composition $Fe_{1.80}Co_{0.20}P$. The quaternary crystal has average dimensions of about $1.50\times0.07\times0.07$ mm^3. The analysis of the EDS spectrum indicates a metal:metalloid ratio of about 2.17:1. This is larger than, yet close to 2:1 (nominal starting composition $Fe_{1.90}Co_{0.10}P_{0.5}Si_{0.65}$) and significantly different from the other alloys eventually forming, usually having 5:3 or 3:1 for the metal:metalloid ratio [27]. Growing crystals of quaternary compounds containing Si therefore turned out more complex than for ternary. Due to the poor solubility of Si in molten tin and the facilitated formation of secondary phases close to Fe_5Si_3 or Fe_3Si, the growth of $Fe_{2-y}Co_yP_{1-x}Si_x$ crystals is challenging and the outcome difficult to anticipate. Starting from a nominal composition leads to collecting a large variety of crystals with a broad range of compositions. Only a few of them present a metal:metalloid ratio close to 2:1 and a needle shape expected for materials having a hexagonal structure. Additional batches of $Fe_{2-y}Co_yP_{1-x}Si_x$ crystals were prepared to cover the targeted composition range, as for the Co-rich $Fe_{1.50\pm0.03}Co_{0.50\pm0.02}P_{0.70\pm0.02}Si_{0.30\pm0.01}$ crystal ($Fe_{1.75}Co_{0.25}P_{0.45}Si_{0.65}$ starting composition) presented hereafter.

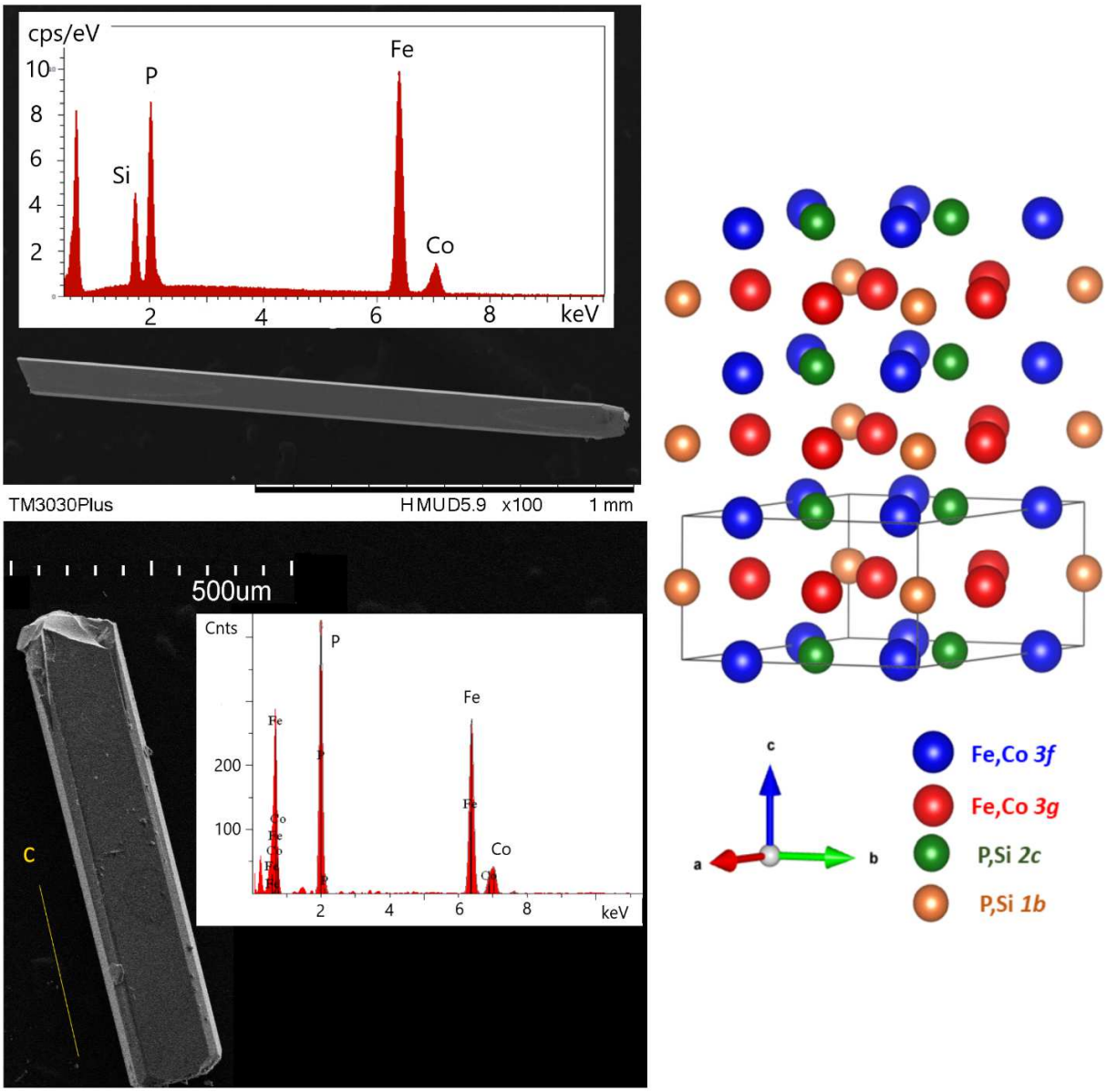

172

173 **Figure 1.** SEM images of as-grown $Fe_{1.94\pm0.06}Co_{0.10\pm0.01}P_{0.61\pm0.02}Si_{0.33\pm0.01}$ (top) and

174 $Fe_{1.78\pm0.04}Co_{0.23\pm0.01}P_{0.98\pm0.02}$ (bottom) single crystals. The insets illustrate the corresponding

175 chemical analysis by EDS. On the right, crystal structure representation of hexagonal

176 $(Fe,Co)_2(P,Si)$ alloys. The basic unit cell (solid contour) was tripled along the *c* direction to

177 highlight the stacking of layers containing inequivalent *3f* and *3g* metal sites along the *c* axis.

178

3.2 Large magnetocrystalline anisotropy in $Fe_{2-y}Co_yP_{1-x}Si_x$ single crystals

In order to highlight the interest in quaternary $Fe_{2-y}Co_yP_{1-x}Si_x$ compounds in comparison to binary Fe_2P or ternary $(Fe,Co)_2P$, we selected three representative crystals for the exploration of the magnetic properties. First, the ternary $Fe_{1.78}Co_{0.23}P_{0.98}$ crystal serves as comparative example illustrating the influence of Co for Fe substitution in Fe_2P. We recall that this composition is one of the highest Co contents achievable prior to the appearance of the orthorhombic structure in ternary $(Fe,Co)_2P$ [11]. The second crystal $Fe_{1.94}Co_{0.10}P_{0.61}Si_{0.33}$ is a quaternary sample with limited Co for Fe and Si for P substitutions. The third $Fe_{1.50}Co_{0.50}P_{0.70}Si_{0.30}$ crystal illustrates the properties of quaternary compounds with a higher Co content.

Figure 2 presents the magnetization curves of the three crystals at room temperature (T = 300 K) recorded parallel and perpendicular to the long axis of the needle, which is the crystallographic *c* axis. We first note that no significant hysteresis can be distinguished between magnetization and demagnetization curves of the present single crystals. Then, even though the uncertainty in the normalized magnetization is relatively large (of the order of 10%), as relying on volume of crystals estimated from SEM, Co for Fe substitution appears to trigger a reduction in magnetization at high Co content. The room temperature data for $Fe_{1.50}Co_{0.50}P_{0.70}Si_{0.30}$ presents a specific saturation magnetization that is approximately 10 A $m^2 kg^{-1}$ lower than that of $Fe_{1.94}Co_{0.10}P_{0.61}Si_{0.33}$. Similarly, the low temperature data (T = 50 K, Supplementary Material), indicate that the specific saturation magnetization of $Fe_{1.78}Co_{0.23}P_{0.98}$ was found to be $m_s \approx 122$ A $m^2 kg^{-1}$ ($J_S \approx 1.06$ T), which is comparable to that of the binary Fe_2P parent. However, larger Co content and Si substitutions trigger a reduction in saturation specific magnetization down to ~90 A $m^2 kg^{-1}$ ($J_S \approx 0.81$ T) for $Fe_{1.50}Co_{0.50}P_{0.70}Si_{0.30}$ at 50 K. In addition, the magnetization saturates to lower values when measured along the hard *c* axis magnetic direction than perpendicular to it. This anisotropy of the saturation magnetization is pronounced at room temperature for the $Fe_{1.94}Co_{0.10}P_{0.61}Si_{0.33}$ crystal

showing the strongest anisotropy prior saturation (approximately 10% at $\mu_0 H$= *3 T)*. A significant anisotropy of the magnetization (~9%) was also reported for the parent Fe_2P composition at 5 K [9], though a smaller anisotropy (~2%) was found for MnFe(P,Si) with the *c* axis as the easy magnetic axis [29]. The anisotropy of the magnetization appears particularly large in Fe_2P-type materials, in particular in comparison to other *3d* metals (usually considered of the order of ~0.1% in Co [32]), and would deserve a dedicated study.

More interesting for applicative purposes is the large magnetic anisotropy before saturation –even at room temperature– exhibited by the three crystals when comparative measurements were performed parallel and perpendicular to the *c* crystallographic axis. In these three cases, the anisotropy fields ($\mu_0 H_A$) are of the order of 2 to 3 T. Yet, we can observe significant differences between the three samples. At room temperature, the two quaternary compounds present a significantly larger anisotropy field than the ternary $Fe_{1.78}Co_{0.23}P_{0.98}$ crystal. This provides a direct confirmation that simultaneous substitutions of Co for Fe and Si for P enables a large magneto-crystalline anisotropy at room temperature in materials deriving from Fe_2P. In addition, the anisotropy field $\mu_0 H_A$ of about 2.8 T for $Fe_{1.94}Co_{0.10}P_{0.61}Si_{0.33}$ is larger than that of the $Fe_{1.50}Co_{0.50}P_{0.70}Si_{0.30}$ crystal with a higher Co content ($\mu_0 H_A \approx 2.5$ T). This reveals the existence of optimal Co and Si contents that maximize the anisotropy field at room temperature, as previously suggested on the basis of theoretical calculations and polycrystalline data [22,27].

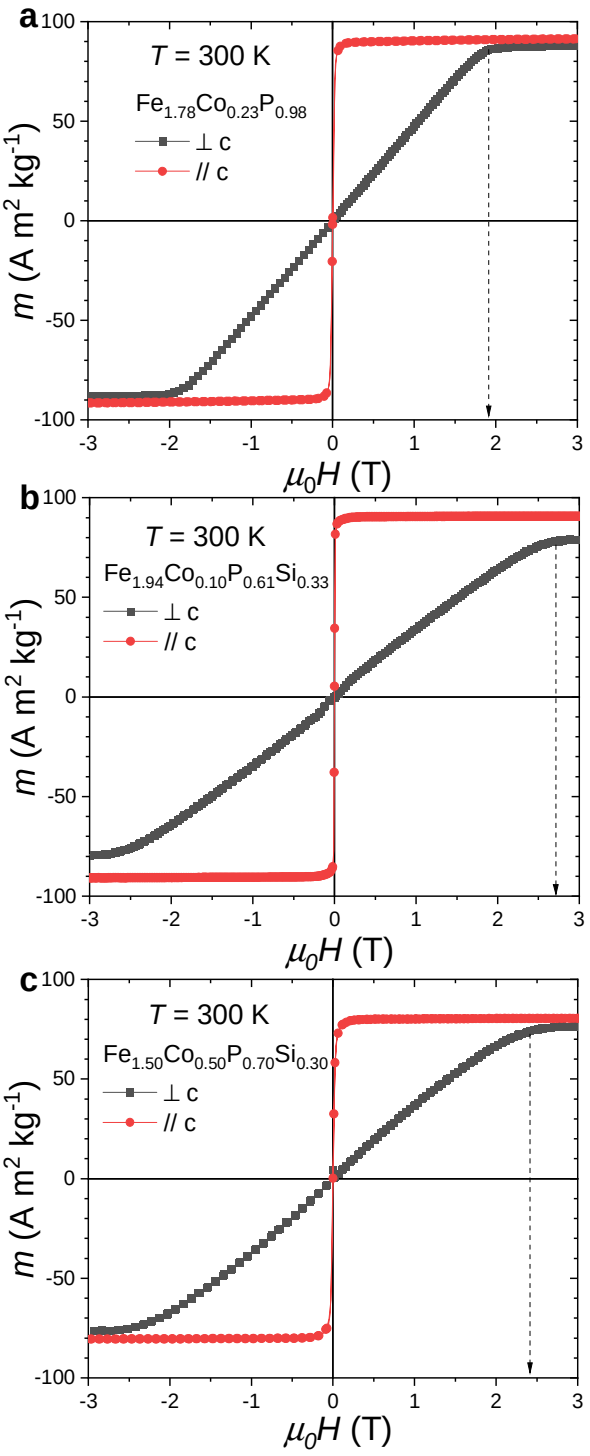

222

223 **Figure 2.** Specific magnetization curves for three $Fe_{2-y}Co_yP_{1-x}Si_x$ single crystals measured
224 parallel and perpendicular to the *c* axis at room temperature (T = 300 K) upon magnetizing and
225 demagnetizing.

To obtain more quantitative information characterizing the magnetic anisotropy, we turn now toward the first- (K_1) and second-order (K_2) anisotropy constants that define the magneto-crystalline anisotropy energy of a hexagonal system, $E \approx K_1 \sin^2\theta + K_2 \sin^4\theta$, where θ is the angle between the direction of the magnetization and the hexagonal *c* axis. The Sucksmith and Thompson method was used to determine K_1 and K_2 from magnetization curves recorded parallel and perpendicular to the *c* direction in the temperature range of 50 - 375 K [33]. **Figure 3** shows the temperature dependence of the anisotropy constants for the three crystals. As expected for materials having an easy *c* axis magnetic anisotropy, K_1 is positive and largely dominant in all three crystals. In this case an alternative estimate of K_1 can be made from the anisotropy field and the saturation magnetization (M_S) by neglecting K_2, resulting in $K_1 \approx \mu_0 H_A M_S/2$ [6]. This alternative method for instance leads to $K_1 \approx 0.9$ MJ m^{-3} for $Fe_{1.94}Co_{0.10}P_{0.61}Si_{0.33}$ at room temperature, which is in good agreement with the Sucksmith and Thompson method ($K_1 \approx 0.87$ MJ m^{-3} and $K_2 \approx 0.09$ MJ m^{-3}). We also note that the present anisotropy constants of single crystals provide a confirmation for former quantitative estimate from oriented powder samples ($K_1 \approx 0.93$ MJ m^{-3} in a closely related $Fe_{1.75}Co_{0.20}P_{0.80}Si_{0.20}$ composition [27]) and for theoretical calculations ($K \approx 0.2$ meV f.u.$^{-1}$ (0.96 MJ m^{-3}) around room temperature for a composition close to $Fe_{1.88}Co_{0.12}P_{0.76}Si_{0.24}$) [22]. At room temperature, the largest magneto-crystalline anisotropy is observed for the $Fe_{1.94}Co_{0.10}P_{0.61}Si_{0.33}$ crystal. At 50 K, the largest anisotropy is found in the ternary $Fe_{1.78}Co_{0.23}P_{0.98}$ crystal with $K_1 \approx 1.81$ MJ m^{-3} ($K_1 \approx 2.03$ MJ m^{-3} at 5 K) which is a very sizable value for a transition-metal based compounds, yet smaller than the Fe_2P binary parent (2.4-2.9 MJ m^{-3}) [9]. In hexagonal symmetry, K_1 is usually considered to scale as $M_S^3(T)$ at low temperature and as $(3/5)M_S^2(T)$ near T_C [6,34], which primarily explains that in $Fe_{1.78}Co_{0.23}P_{0.98}$ the magnetic anisotropy decreases much faster with the temperature than the magnetization and that Curie temperatures much higher than room temperature are required to reach a large room-temperature anisotropy, as achieved in $(Fe,Co)_2(P,Si)$ quaternary alloys. These tendencies allow one to draw the following scenario on the evolution of the magnetic properties as function of chemical

substitutions. The binary parent is likely to be close to the optimum to maximize the magnetic anisotropy at low temperature. Co for Fe and Si for P substitutions increase the Curie temperature, but decrease the ground state magneto-crystalline anisotropy, therefore requiring to mitigate both aspects to reach a large magnetic anisotropy at room temperature. This is also the primary reason why the maximum room-temperature magnetic anisotropy was observed at relatively limited substitutions with Co around 0.2 and Si between 0.2 to 0.25 in the preliminary polycrystalline data [27].

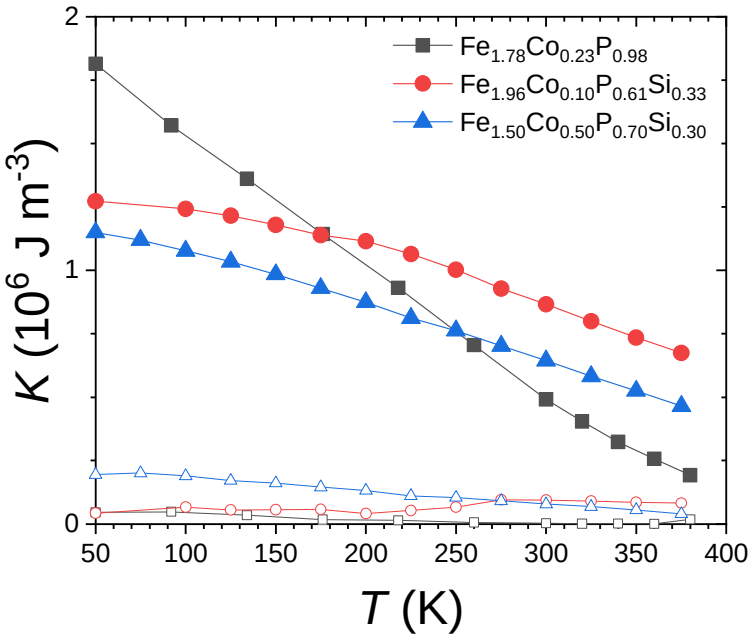

Figure 3. Magneto-crystalline anisotropy constants K_1 (full symbols) and K_2 (open symbols) determined as a function of the temperature by the Sucksmith and Thompson method for the three single crystals.

Table 1 summarizes the magnetic anisotropy parameters of the three crystals and compares it to some candidate rare-earth-free permanent magnets. $(Fe,Co)_2(P,Si)$ materials present a significantly larger magnetic anisotropy and saturation magnetization than ferrites. The magnetocrystalline anisotropy of $(Fe,Co)_2(P,Si)$ remains lower than L_{10} CoPt or FePt permanent

magnet candidates, but Pt containing materials are not economically competitive compared to other magnets, even for rare-earth magnets. $(Fe,Co)_2(P,Si)$ present a magnetocrystalline anisotropy and a saturation magnetization that is comparable to the best Mn-based candidates for rare-earth-free permanent magnets. The magnetic hardness parameter $\kappa = \sqrt{(K_1/\mu_0 M_S^2)}$ is a convenient figure of merits for permanent magnets, with $\kappa > 1$ the threshold for a material to resist to self-demagnetization [6,35]. The room-temperature magnetic hardness parameters for ternary $(Fe,Co)_2P$ and quaternary $(Fe,Co)_2(P,Si)$ alloys are about 1.0 and 1.3, respectively. This further supports that these materials are potential hard magnetic materials, and the larger κ for quaternaries highlights their increased interest compared to the ternary alloys. Overall, by combining a high Curie temperature, a large magnetic anisotropy and a relatively large saturation magnetization, the $(Fe,Co)_2(P,Si)$ system is highly promising for permanent magnet applications and would suitably fit in the performance gap between ferrites and rare-earth magnets.

Table 1. Comparison of the main anisotropy constant (K), saturation specific magnetization (m_s), saturation magnetic polarization (J_s), magnetic hardness parameter (κ, calculated for the present samples using anisotropy constants and saturation magnetizations at 300 K), and magnetic transition temperature (T_{tr}) between the present crystals, representative ferrites and some rare-earth-free permanent magnet candidates.

Material	K (50 K) [MJ m^{-3}]	K (300 K) [MJ m^{-3}]	m_S (50 K) [A m^2 kg^{-1}]	J_s [T]	κ (300 K)	T_{tr} [K]	Ref.
$Fe_{1.78}Co_{0.23}P_{0.98}$	1.81	0.50	122	1.06 (50 K)	1.0	412	present
$Fe_{1.94}Co_{0.10}P_{0.61}Si_{0.33}$	1.28	0.87	101	0.88 (50 K)	1.3	560	present
$Fe_{1.50}Co_{0.50}P_{0.70}Si_{0.30}$	1.15	0.65	90	0.81 (50 K)	1.3	535	present
Fe_2P	2.2	-	125	1.05 (50 K)	-	214	[7-9]
$BaFe_{12}O_{19}$	0.45	0.33	92	0.48	1.35	725	[35,36]
$SrFe_{12}O_{19}$	-	0.35	90	0.45	1.2	732	[35,37]
MnBi	-0.2	1.1	62	0.73	1.46	628	[35,38]
MnAl	1.7	1.2	110	0.75	1.95	620	[35,39]
CoPt	4.9	4.1	55	1.01	2.47	840	[35,40]
FePt	7.4	6.0	90	1.43	2.02	660	[6,41]

3.3 Top-down synthesis of $Fe_{2-y}Co_yP_{1-x}Si_x$ submicron-sized particles

$(Fe,Co)_2(P,Si)$ materials do not present significant coercive field in single crystals or bulk polycrystalline materials due to the formation of a magnetic multidomain configuration. One approach to induce hard magnetic properties can be to restore a single domain structure by reducing the particle size. The maximum single domain size for an isolated particle can be estimated as $R_{sd} \approx 36(AK_1)^{1/2}/\mu_0 M_S^2 \approx 150$ nm, with A the exchange stiffness parameter, which is usually of the order of 10 pJ m^{-1} for transition metal ferromagnets with a Curie temperature well above room temperature [6]. This maximum single domain size is comparable to other permanent magnetic materials (about 270 nm in ferrites and 110 nm in $Nd_2Fe_{14}B$) [6]. The smallest width of the stripes observed in MFM microscopy was about 200 nm (Supplemental Material Figure S3), which is comparable to the theoretical estimate. Both estimates indicate that the single domain size corresponds to the range of relatively large particles, which can be obtained by top down methods. $Fe_{2-y}Co_yP_{1-x}Si_x$ submicron-sized particles were therefore synthesized by ball-milling of bulk polycrystalline samples. While ball-milling usually leads to the development of microstrains, crystallite agglomeration and results in irregular particle shapes of variable size, for this first exploration of $(Fe,Co)_2(P,Si)$ particles it was the preferred method as it allows a good control of the chemical composition. Different milling methods were explored including vibratory ball-milling, dry planetary ball-milling and wet planetary ball-milling with surfactant. All these methods led to the synthesis of submicron-sized particles with an appreciable coercive field. We hereafter focus on presenting materials prepared by dry planetary ball-milling, as this method is the most straightforward to scale-up.

Figure 4 presents powder X-ray diffraction patterns of $Fe_{1.75}Co_{0.20}P_{0.75}Si_{0.25}$ submicron-sized particles prepared by ball milling of polycrystalline material. The starting polycrystalline material presents a diffraction pattern typical for the Fe_2P-type hexagonal crystal structure. A minor contamination from a secondary phase having a 5:3 metal:metalloid ratio can however be

distinguished (<4 wt.%). Increasing the milling time leads to a significant peak broadening up to 8 h milling, then it saturates. The three most intense peaks of the Fe_2P-type phase (111), (201) and (210) from 40.3° to 47.2° remain independent allowing an estimation of the crystallite size (d) using the Sherrer's equation $d = k\lambda/\beta\cos\theta$, where k is a constant that dependents on the crystallite shape and the definition of an average diameter, usually taken as k = 0.9, λ is the X-ray wavelength, and β is the broadening of the (111) diffraction peak. Additional sources of peak broadening were not considered in first approximation. In particular, the development of (micro)strains was not accounted for since, at the exception of the (210) peak presenting a small shift to lower angles, no significant changes in peak positions could be observed. Ball milling leads to a progressive crystallite size reduction down to about 20 nm after 8 h of milling. Similar crystallite sizes were obtained when preparing submicrometric particles of MnFe(P,Si) giant magnetocaloric materials by ball milling [42]. Increasing the milling time further does not lead to a significant further reduction in crystallite size. Very long milling, *e.g.* 48 h, however results in the appearance of a broad bump around 18°, indicating the appearance of an amorphous phase. From the point of view of reaching a large coercive field without compromising the saturation magnetization by the formation of an amorphous phase, the optimal milling time is therefore expected to be in the range of 5 - 16 h. Using the same mill (planetary ball mill with same rotary milling speed, jars size and ball mass), but polycrystalline materials dispersed in heptane solvent with oleic acid surfactant (wet milling) results in similar crystallite sizes and magnetic coercivity. This indicates that the presently obtained crystallite size is partly limited by the milling energy. In addition, SEM imaging of the ball-milled product (Supplementary material) revealed a very broad particle size distribution ranging from crystallites of less than 100 nm up to 40 µm particles formed by the agglomeration of (sub)micrometer-sized crystallites.

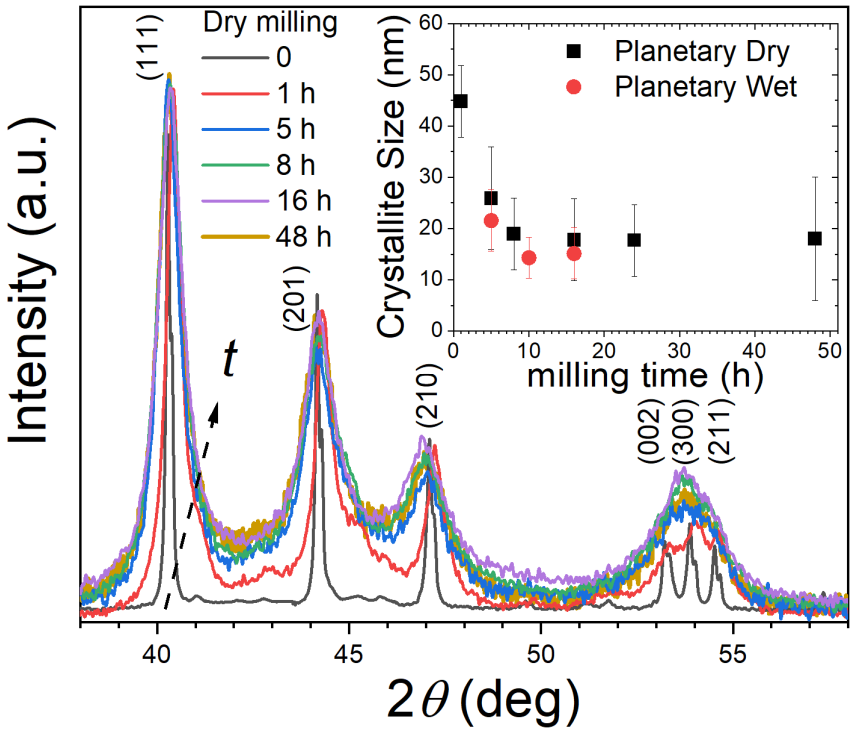

Figure 4. Structure $Fe_{1.75}Co_{0.20}P_{0.75}Si_{0.25}$ submicron-sized particles. The X-ray diffraction patterns of dry ball-milled $Fe_{1.75}Co_{0.20}P_{0.75}Si_{0.25}$ powders with increasing milling times of 1, 5, 8, 16 and 48 h are compared to that of hand-crushed polycrystalline material. The patterns were subtracted for background and normalized to highlight the peak broadening. The inset presents the crystallite size estimated with the Sherrer's equation using the (111) reflection.

Although $(Fe,Co)_2(P,Si)$ submicron-sized particles should be considered as a flammable solid, we note that they are relatively stable. The presently reported particles were stored in a glovebox employing a purified Ar atmosphere. But additional batches stored in air for a long period of time (6 months) did not present a noticeable deterioration of their crystal structure, nor of their magnetic properties.

3.4 Permanent magnetic properties of bounded $Fe_{2-y}Co_yP_{1-x}Si_x$ submicron-sized particles

Magnetization hysteresis cycles were recorded for $Fe_{1.75}Co_{0.20}P_{0.75}Si_{0.25}$ submicron-sized particles milled in different conditions and bonded with epoxy resin. **Figure 5** presents the evolution of the

coercive field as a function of the milling time for different milling conditions. The largest coercive fields are achieved for 8-16 h of milling. Additional magnetization cycles for 16 h milling (including the virgin magnetization curve) are shown in **Figure 6** and in Supplementary material. While coercive fields of $\mu_0 H_c \approx 70$ mT (55 kA m^{-1}) at room temperature remain modest in comparison to rare-earth magnets, it clearly demonstrates that permanent magnetic properties can be obtained in $(Fe,Co)_2(P,Si)$ quaternary alloys with the Fe_2P-type structure. ~~This shape is often considered as a signature of pinning-type coercivity [6,34], but is not a conclusive feature here as the samples might be formed of particles less than the critical size of a single domain. Two additional observations nevertheless suggest that pinning might be the dominant coercivity mechanism: *i)* coercivity is presently observed in ball-milled samples only, a technique known to cause in addition to surface stresses, large amount of structural and microstructural defects (vacancies and/or dislocations) which may act as pinning centers; *ii)*~~ The highest coercive field achieved so far in $(Fe,Co)_2(P,Si)$ quaternary alloys ($\mu_0 H$c ≈ 0.14 T, Supplementary material) was actually observed in $Fe_{1.85}Co_{0.1}P_{0.6}Si_{0.4}$ particles showing a two phase mixture of Fe_2P-type and orthorhombic BCO-type structures. ~~, for which the significant secondary phase content can be expected to provide further pinning centers and enhance the coercivity.~~ The lower value of the room-temperature coercivity of $Fe_{1.75}Co_{0.20}P_{0.75}Si_{0.25}$ submicron-sized particles compared to the value reported for $Fe_{1.7}Co_{0.3}P$ powders ($\mu_0 H_c \approx 0.2$ T [10]) primarily originates from the difference in synthesis methods, the lixiviating method yielding fine, relatively well dispersed, particles directly after leaching. Similarly ultrafine particles of $(Fe,Co)_2P$ ternary alloys (in the range 100 to 20 nm) prepared by a gas phase reaction were found to reach a coercive field up to 0.32 T at room temperature [16]. When comparing $Fe_{1.80}Co_{0.20}P$ ($\mu_0 H_c \approx 30$ mT, Supplementary material) and $Fe_{1.75}Co_{0.20}P_{0.75}Si_{0.25}$ submicrometric particles synthesized in similar conditions, the coercivity of the quaternary alloys is significantly larger. This confirms that: (*i*) quaternary $(Fe,Co)_2(P,Si)$ alloys are more promising for permanent magnets than ternary $(Fe,Co)_2P$ alloys and (*ii*) the optimal synthesis conditions maximizing the coercivity of ternary or quaternary alloys deriving

375 from Fe_2P have not yet been reached by the present top down ball-milling approach, so that a
376 significant improvement of the coercivity is likely to be achievable. Recalling that the Sherrer's
377 equation estimates the crystallite size and therefore tends to underestimate the real particle size
378 and does not account for agglomeration during milling, our present particles do not have the
379 optimal shape to reach the full potential of $(Fe,Co)_2(P,Si)$ alloys for permanent magnetic
380 applications. We can nevertheless note that $(Fe,Co)_2(P,Si)$ quaternary alloys show higher Curie
381 temperatures than $(Fe,Co)_2P$ ternary alloys [16,19] and therefore their permanent magnetic
382 properties are preserved up to higher temperatures (up to about 480 K for the present sample,
383 Figure 5).

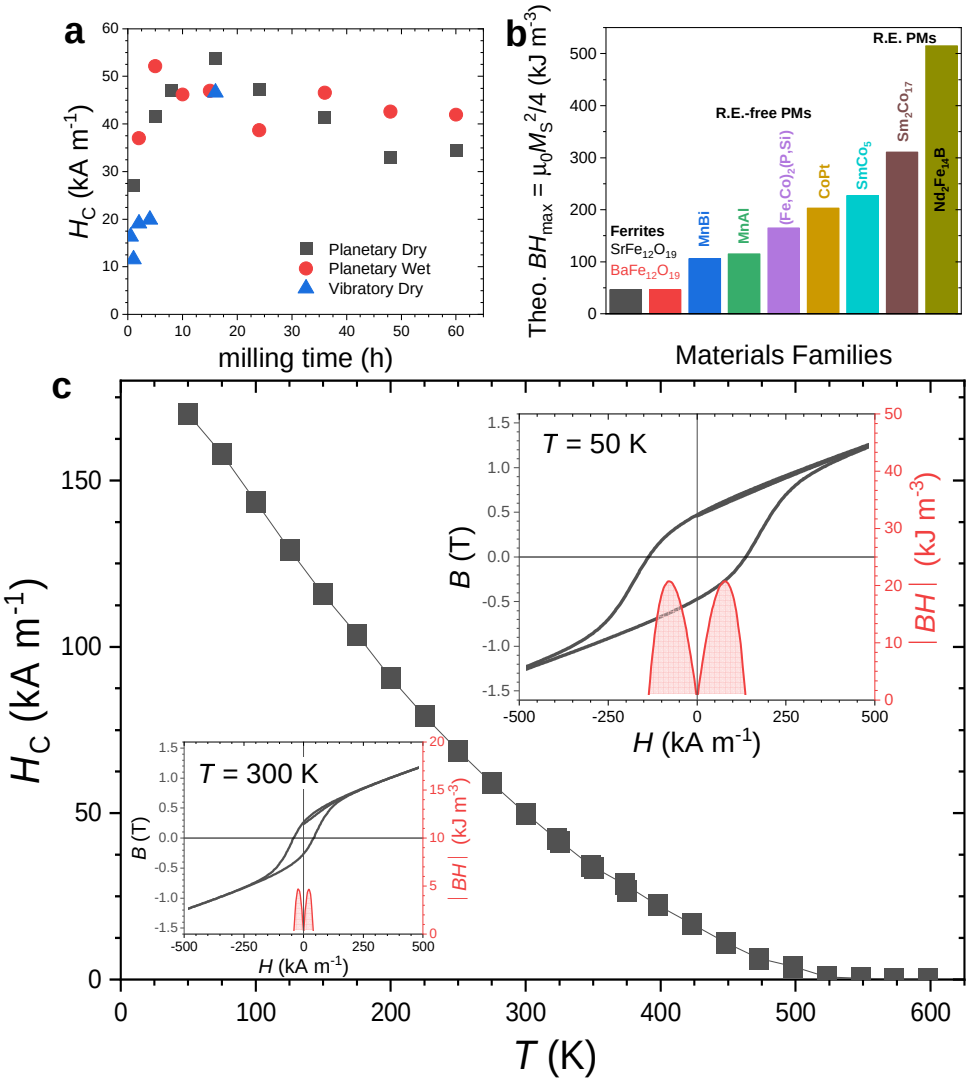

384

385 **Figure 5.** Permanent magnetic properties of $Fe_{1.75}Co_{0.20}P_{0.75}Si_{0.25}$ submicron-sized particles.
386 (a) Coercive field (H_c) as a function of milling time for different milling conditions. (b) Theoretical
387 $|BH|_{max}$ energy product estimated from the saturation magnetization for different families of
388 permanent magnets. (c) Temperature dependence of the coercive field for $Fe_{1.75}Co_{0.20}P_{0.75}Si_{0.25}$
389 submicron-sized particles synthesized by 16 h of planetary ball milling (bonded oriented
390 powders). The insets present the $B(H)$ hysteresis measurements at 50 and 300 K.

391 When considering the theoretical $|BH|_{max}$, which can be calculated from the saturation
392 magnetization as $\mu_0 M_S^2/4 \approx 165$ kJ m^{-3} [6], we can see that $(Fe,Co)_2(P,Si)$ materials are an

interesting intermediate between the high $|BH|_{max}$ of rare-earth magnets and the low performance of ferrites (Figure 5b). In particular, the theoretical $|BH|_{max}$ of $(Fe,Co)_2(P,Si)$ is significantly larger (about +40%) than that of other candidates for rare-earth-free magnets, such as MnBi or MnAl. The experimental $|BH|_{max}$ obtained in the present $Fe_{1.75}Co_{0.20}P_{0.75}Si_{0.25}$ submicrometric particles bonded by epoxy resin and oriented in a $\mu_0 H$ = 1.1 T magnetic field range from about 21 kJ m^{-3} at 50 K (~12% of the theoretical $|BH|_{max}$) to about 5 kJ m^{-3} at room temperature. These energy products are still small compared to the theoretical ones or compared to the well-established permanent magnetic materials. These low performances are partially due to the imperfect orientation process, the energy products for the oriented bonded samples were found to be only ~20% higher than the corresponding isotropic bonded sample, which may be due to particles agglomeration during milling. But they are already comparable to that of ferrite magnets (of the order of 15 kJ m^{-3} for oriented bonded ferrites and 5 kJ m^{-3} for isotropic bonded ferrites) [6]. The magnetic hardness parameters obtained in section 3.2 ($\kappa \approx 1.3$) settles $(Fe,Co)_2(P,Si)$ amongst hard magnetic materials, for which a more significant fraction of the theoretical $|BH|_{max}$ should be achievable. It often takes a long struggle from the introduction of a new hard magnetic composition to reach its full potential as permanent magnet. As mentioned above for the coercive field, significant improvements of the experimental $|BH|_{max}$ can be expected by optimizing the material synthesis and magnet preparation conditions.

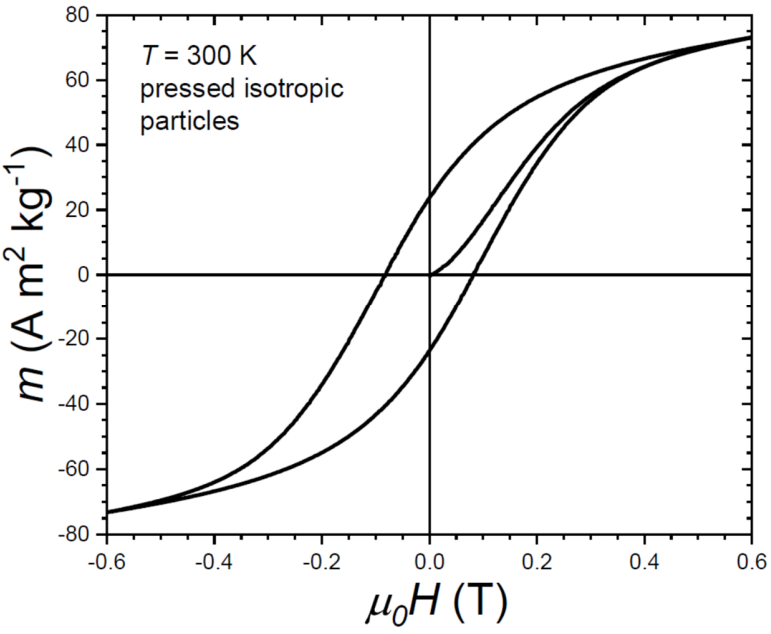

Figure 6. Magnetization cycle including the initial magnetization branch at T = 300 K of isotropically pressed $Fe_{1.75}Co_{0.20}P_{0.75}Si_{0.25}$ submicron-sized particles prepared by 16 h dry milling.

4. Conclusions

Ternary $(Fe,Co)_2P$ and quaternary $(Fe,Co)_2(P,Si)$ alloys were successfully prepared in single crystal form and their magnetic properties were investigated. Compared to the binary parent Fe_2P, substitutions with Co or Si decrease the magneto-crystalline anisotropy at low temperature, but increase the Curie temperature. As a result, the magneto-crystalline anisotropy at room temperature is enhanced in $(Fe,Co)_2(P,Si)$ quaternary alloys. The present $Fe_{1.94}Co_{0.10}P_{0.61}Si_{0.33}$ single crystal shows the largest magneto-crystalline anisotropy of $K_1 \approx 0.9$ MJ m^{-3} at room temperature, which brings support to former preliminary polycrystalline data, and confirms that $(Fe,Co)_2(P,Si)$ show a much stronger magnetic anisotropy than ferrites. $(Fe,Co)_2(P,Si)$ submicron-sized particles were synthesized by a top-down ball-milling approach and their magnetization was recorded. For the first time, hard magnetic properties were observed in $(Fe,Co)_2(P,Si)$ quaternary

alloys. While the coercive field and energy products are nearly comparable with ferrites, they so far remain modest in comparison to other well-established permanent magnetic materials. Yet further improvements of the performances are anticipated by optimization of the synthesis conditions. Owing to the high economical interest that a permanent magnet essentially made of iron and abundant metalloid elements has, $(Fe,Co)_2(P,Si)$ quaternary alloys are promising rare-earth-free permanent magnet materials that deserve further investigation.

Acknowledgments

The work is supported by the Inner Mongolia Normal University (grant numbers 2018YJRC002 and 2018YJRC003), the Inner Mongolia Autonomous Region (grant numbers NJZY20025 and NJYT-20-A17) and the National Natural Science Foundation of China (grant numbers 11904188 and 51961033).

References

[1] J. M. D. Coey, Perspective and Prospects for Rare Earth Permanent Magnets, Engineering 2020, 6, 119-131.

[2] O. Gutfleisch, M. A. Willard, E.Brück, C. H. Chen, S. G. Sankar, J. P. Liu, Magnetic Materials and Devices for the 21st Century: Stronger, Lighter, and More Energy Efficient, Adv. Mater. 2011, 23, 821-842.

[3] J. Cui, M. Kramer, L. Zhou, F. Liu, A. Gabay, G. Hadjipanayis, B. Balasubramanian, D. Sellmyer, Current Progress and Future Challenges in rare-earth-free Permanent Magnets, Acta Mater. 2018, 158, 118-137.

[4] J. M. D. Coey, Permanent magnets: Plugging the gap, Scripta Mater. 2012, 67, 524-529.

[5] A. K. Pathak, M. Khan, K. A. Gschneidner Jr., R. W. McCallum, L. Zhou, K. Sun, K. W. Dennis, C. Zhou, F. E. Pinkerton, M. J. Kramer, V. K. Pecharsky, Cerium: An Unlikely Replacement of Dysprosium in High Performance Nd–Fe–B Permanent Magnets, Adv. Mater. 2015, 27, 2663-2667.

[6] J. M. D. Coey, Magnetism and Magnetic Materials, Cambridge University Press, Cambridge, UK, 2019.

[7] H. Fujii, T. Hokabe, T. Kamigaichi, T. Okamoto, Magnetic Properties of Fe_2P Single Crystal, J. Phys. Soc. Jpn. 1977, 43, 41-46.

[8] L. Lundgren, G. Tarmohamed, O. Beckman, B. Carlsson, S. Rundqvist, First Order Magnetic Phase Transition in Fe_2P, Phys. Scripta 1978, 17, 39-48.

[9] L. Caron, M. Hudl, V. Höglin, N. H. Dung, C. P. Gomez, M. Sahlberg, E. Brück, Y. Andersson, P. Nordblad, Magnetocrystalline Anisotropy and the Magnetocaloric Effect in Fe_2P, Phys. Rev. B 2013, 88, 094440.

[10] K. J. de Vos, W. A. J. J. Velge, M. G. van der Steeg, H. Zijlstra, Permanent Magnetic Properties of Iron‐Cobalt‐Phosphides, J. Appl. Phys. 1962, 33, 1320-1322.

[11] R. Fruchart, A. Roger, J. P. Senateur, Crystallographic and Magnetic Properties of Solid Solutions of the Phosphides M_2P, M = Cr, Mn, Fe, Co, and Ni, J. Appl. Phys. 1969, 40, 1250-1257.

[12] H. Fujii, T. Hokabe, T. Kamigaichi, H. Fujiwara, T. Okamoto, Magnetic Properties of Single Crystals of the System $(Fe_{1-x}Ni_x)_2P$, J. Phys. Soc. Jpn. 1978, 44, 96-100.

[13] R. Chandra, S. Bjarman, T. Ericsson, L. Häggström, C. Wilkinson, R. A. Wäppling, Mössbauer and X-ray Study of $Fe_2P_{1-x}B_x$ Compounds ($x < 0.15$), J. Solid State Chem. 1980, 34, 389-396.

[14] P. Jernberg, A. A. Yousif, L. Häggström, Y. Andersson, A Mössbauer study of $Fe_2P_{1-x}Si_x$ ($x \leq 0.35$), J. Solid State Chem. 1984, 53, 313-322.

[15] A. Catalano, R. J. Arnott, A. Wold, Magnetic and Crystallographic Properties of the System $Fe_2P_{1-x}As_x$, J. Solid State Chem. 1973, 7, 262-268.

[16] Y. Tokuoka, J. Yoshinari, Ferromagnetic ultrafine Particles, Method of Making, and Recording Medium using the same. US patent US005256479A, 1993.

[17] A. Mendoza-Garcia, H. Zhu, Y. Yu, Q. Li, L. Zhou, D. Su, M. J. Kramer, S. Sun, Controlled Anisotropic Growth of Co-Fe-P from Co-Fe-O Nanoparticles, Angew. Chem. Int. Ed. 2015, 54, 9642.

[18] W. Yang, X. Wu, Y. Yu, C. Yang, S. Xu, H. Li, Controlled Synthesis and Magnetic Properties of Iron–Cobalt–Phosphide Nanorods, Nanoscale 2016, 8, 16187-16191.

[19] D. Li, M. P. Arachchige, B. Kulikowski, G. Lawes, T. Seda, S. L. Brock, Control of Composition and Size in Discrete $Co_xFe_{2-x}P$ Nanoparticles: Consequences for Magnetic Properties, Chem. Mater. 2016, 28, 3920-3927.

[20] E. K. Delczeg-Czirjak, Z. Gercsi, L. Bergqvist, O. Eriksson, L. Szunyogh, P. Nordblad, B. Johansson, L. Vitos, Magnetic Exchange Interactions in B-, Si-, and As-doped Fe_2P from First-Principles Theory, Phys. Rev. B 2012, 85, 224435.

[21] M. Costa, O. Grånäs, A. Bergman, P. Venezuela, P. Nordblad, M. Klintenberg, O. Eriksson, Large Magnetic Anisotropy of Fe_2P Investigated via ab initio Density Functional Theory Calculations, Phys. Rev. B 2012, 86, 085125.

[22] I. A. Zhuravlev, V. P. Antropov, A. Vishina, M. van Schilfgaarde, K. D. Belashchenko, Tunable Dimensional Crossover and Magnetocrystalline Anisotropy in Fe_2P-based Alloys, Phys. Rev. Materials 2017, 1, 051401(R).

[23] O. Tegus, E. Brück, K. H. J. Buschow, F. R. de Boer, Transition-metal-based magnetic refrigerants for room-temperature applications, Nature 415 (2002) 150–152.

[24] D. Liu, M. Yue, J. Zhang, T. M. McQueen, J. W. Lynn, X. Wang, Y. Chen, J. Li, R. J. Cava, X. Liu, Z. Altounian, Q. Huang, Origin and tuning of the magnetocaloric effect in the magnetic refrigerant $Mn_{1.1}Fe_{0.9}(P_{0.8}Ge_{0.2})$, Phys. Rev. B 79 (2009) 014435.

[25] N. H. Dung, Z.Q. Ou, L. Caron, L. Zhang, D.T. Cam Thanh, G.A. de Wijs, R.A. de Groot, K.H.J. Bushow, E. Brück, Mixed Magnetism for Refrigeration and Energy Conversion, Adv. Energy Mater. 1 (2011) 1215–1219.

[26] M. Fries, L. Pfeuffer, E. Bruder, T. Gottschall, S. Ener, L. V. B. Diop, T. Gröb, K. P. Skokov, O. Gutfleisch, Microstructural and magnetic properties of Mn-Fe-P-Si (Fe2 P-type) magnetocaloric compounds, Acta Materialia 132 (2017) 222-229.

[27] F. Guillou, Sun-Liting, O. Haschuluu, Z. Q. Ou, E. Brück, O. Tegus, H. Yibole, Room Temperature Magnetic Anisotropy in Fe_2P-Type Transition Metal Based Alloys, J. Alloys Compd. 2019, 800, 403-411.

[28] J. Y. Xu, Lingling-Bao, H. Yibole, F. Guillou, Structure and Magnetic Properties of $Fe_{1.95-x}Ni_xP_{1-y}Si_y$ Alloys, Solid State Commun. 2020, 319, 113996.

[29] H. Yibole, F. Guillou, Y. K. Huang, G. R. Blake, A. J. E. Lefering, N. H. van Dijk, E. Brück, First-order Ferromagnetic Transition in Single-crystalline $(Mn,Fe)_2(P,Si)$, Appl. Phys. Lett. 2015, 107, 162403.

[30] J. Rodríguez-Carvajal, Recent Advances in Magnetic Structure Determination by Neutron Powder Diffraction, Physica B: Condens. Matter 1993, 192, 55-69.

[31] K. Momma, F. Izumi, VESTA 3 for three-dimensional visualization of crystal, volumetric and morphology data, J. Appl. Crystallogr. 2011, 44, 1272-1276.

518 [32] E. R. Callen and H. B. Callen, Anisotropic Magnetization, J. Phys. Chem. Solids 1960, 16,
519 310.

520 [33] W. Sucksmith, F. R. S. Thompson, J. E. Thompson, The Magnetic Anisotropy of Cobalt,
521 Proc. Royal Soc. A 1954, 225, 362-375.

522 [34] É. du Trémolet de Lacheisserie, D. Gignoux, M. Schlenker, Magnetism, Springer, New
523 York, NY, 2005.

524 [35] R. Skomski, J. M. D. Coey, Magnetic anisotropy — How much is enough for a permanent
525 magnet? Scripta Mater. 2016, 112, 3-8.

526 [36] J. Wang, F. Zhao, W. Wu, G. M. Zhao, Unusual Temperature Dependence of the Magnetic
527 Anisotropy Constant in Barium Ferrite $BaFe_{12}O_{19}$, J. Appl. Phys. 2011, 110, 096107.

528 [37] R. C. Pullar, Hexagonal Ferrites: a Review of the Synthesis, Properties and Applications of
529 Hexaferrite Ceramics, Prog. Mater. Sci. 2012, 57, 1191-1334.

530 [38] B. W. Roberts, Neutron Diffraction Study of the Structures and Magnetic Properties of
531 Manganese Bismuthide, Phys. Rev. 1956, 104, 607.

532 [39] L. Pareti, F. Bolzoni, F. Leccabue, A. E. Ermakov, Magnetic Anisotropy of MnAl and MnAlC
533 Permanent Magnet Materials, J. Appl. Phys. 1986, 59, 3824.

534 [40] H. Shima, K. Oikawa, A. Fujita, K. Fukamichi, K. Ishida, S. Nakamura, T. Nojima,
535 Magnetocrystalline Anisotropy Energy in L10-type CoPt Single Crystals, J. Magn. Magn. Mater.
536 2005, 290–291, 566-569.

537 [41] K. Inoue, H. Shima, A. Fujita, K. Ishida, K. Oikawa, K. Fukamichi, Temperature
538 Dependence of Magnetocrystalline Anisotropy Constants in the Single Variant State of L10-
539 Type FePt Bulk Single Crystal, Appl. Phys. Lett. 2006, 88, 102503.

[42] N. V. Thang, N. H. van Dijk, E. Brück, Effects of Milling Conditions on Nano-scale MnFe(P,Si) Particles by Surfactant-assisted High-energy Ball Milling, Phys. Procedia 2015, 75, 1104-1111.